

1 **SUPPLEMENT**

2 **Methods**

3 *Flow Cytometry*

4 Gates were drawn on CD45⁺ leukocytes by doublet exclusion (forward scatter height vs forward
5 scatter area; side scatter height vs side scatter area) and dead cell exclusion using fixable
6 viability dyes. Live lymphocytes size gates were further defined with sequential gating on the
7 CD3⁺ T cell population, followed by CD4⁺ and CD8⁺ T subset gating. Among CD4⁺ T cells,
8 Foxp3⁺ CD25⁺ cells were defined as regulatory (Treg) cells. NK cells were defined as CD45⁺
9 CD3⁻CD335⁺ CD49b⁺ cells. G-MDSC was defined as CD45⁺ CD11b⁺ I-A/I-E⁻ Ly6G⁺ Ly6C⁻
10 cells, M-MDSC was defined as CD45⁺ CD11b⁺ I-A/I-E⁻ F4/80⁻ Ly6C⁺ Ly6G⁻ cells, and
11 macrophages were defined as CD45⁺ CD11b⁺ I-A/I-E⁺ F4/80⁺ Ly6C⁻ cells as previously
12 described(19). Cells that did not fall within the MDSC (both G-MDSCs and M-MDSCs) and
13 macrophage gates were designated as “undefined CD11b⁺” myeloid cells. Fluorescence minus
14 one, unstained, and isotype controls were included for assessment of surface and intracellular
15 proteins. The percentage of each cell subset within viable CD45⁺ cells or total live cells in the
16 tumor was calculated. The following antibodies and clones were used: CD45 (30-F11), CD11b
17 (M1/70), CD8 (53-6.7), Ly6G (1A8), F4/80 (BM8), Ly6C (AL-21), I-A/I-E (M5/114.15.2),
18 CD11c (N418), CD3e (145-2C11), CD4 (GK1.5), CD49b (DX5), CD335 (29A14), CD25
19 (PC61) FOXP3 (MF-14), TCRβ (H57-597), and GR-1 (clone RB6-8C5). All antibodies were
20 purchased from BioLegend or BD Biosciences.

21 *Immunohistochemistry*

22 Sections were cut from formalin-fixed paraffin-embedded tissue blocks at 5 μm, baked at 60°C
23 for 60 minutes, then deparaffinized and rehydrated with serial passage through changes of xylene

24 and graded ethanols. All slides were subjected to heat-induced epitope retrieval for 4 minutes at
25 120°C in a Decloaking Chamber (Biocare Medical) in 1× Target Retrieval Solution (Agilent).
26 Endogenous peroxidase in tissue was blocked by incubation of slides in 3% hydrogen peroxide
27 solution before incubation with primary antibody (anti–mouse CD3, clone CD3-12 [AbD
28 Serotec]) for 60 minutes. Antigen-antibody binding was detected through the application of
29 Rabbit Anti–Rat IgG (Abcam) and ImmPRESS HRP Horse Anti–Rabbit IgG Polymer Detection
30 Kit (Vector), followed by application of 3,3’ diaminobenzidine chromogen (Agilent). Stained
31 slides were counterstained with hematoxylin and coverslipped for review.

32 ***RNA extraction and targeted RNA profiling***

33 For tumor tissue RNA isolation, organs were homogenized into RNA STAT-60 (Tel-Test Inc.)
34 using a polytron homogenizer, after which total RNA was extracted according to the
35 manufacturer's instructions. After isopropanol precipitation, total RNA was reextracted with
36 phenol/chloroform/isoamyl alcohol (25:24:1; Sigma-Aldrich) using phase-lock light tubes
37 (ThermoFisherScientific). DNase-treated total RNA was reverse-transcribed using QuantiTect
38 Reverse Transcription (Qiagen) according to the manufacturer's instructions. 20× primer assays
39 were obtained commercially from ThermoFisherScientific. Gene-specific preamplification was
40 performed on 10 ng cDNA according to the manufacturer's instructions (Biomark; Fluidigm).
41 Real-time quantitative polymerase chain reaction (PCR) was then performed on the Biomark
42 (Fluidigm) using 20× TaqMan primer assays (ThermoFisherScientific) with TaqMan Universal
43 PCR Master Mix with no AmpErase UNG. Samples and primers were run on BioMark 96.96
44 Dynamic Arrays according to the manufacturer's instructions (Fluidigm). Ubiquitin levels were
45 measured in a separate reaction and were used to normalize the data by the ΔC_t method. Using

46 the mean cycle threshold value for ubiquitin and the gene of interest for each sample, the
47 equation $1.8^{(Ct \text{ ubiquitin} - Ct \text{ gene of interest})} \times 10^4$ was used to obtain the normalized values.

48 ***RNA-sequencing***

49 RNA-sequencing was performed using purified total RNA as previously described (1) and the
50 TruSeq stranded total RNA RiboZero library preparation kit (catalog no. RS-122-2201)
51 according to the manufacturer's instructions (Illumina). The resultant cDNA libraries were
52 sequenced on Illumina HiSeq™ 4000 using a 50 base paired-end run. Cleaned reads were
53 aligned to the Mouse.B38 genome reference using the Omicsoft Aligner (Qiagen) with ≤ 2
54 allowed mismatches. Gene-level raw counts and fragments per kilobase million (FPKM) were
55 determined by the OSA algorithm as implemented in Omicsoft Array Studio (v10.0.1.118) and
56 using Ensembl.R93 gene models. Approximately 90% of reads across all samples mapped to the
57 reference genome (corresponding to 40-160 million reads). Gene count normalization and
58 differential expression analysis were performed based on modeling the raw counts within the
59 framework of a negative binomial model using the R package DESeq2 (v1.22.2) yielding fold
60 change and corrected *P* values (False Discovery Rate, Benjamini–Hochberg; FDR_BH). Samples
61 from vehicle-treated animals were used as baseline for muDX400 treatment comparisons. The
62 muDX400 differentially expressed genes (DEG) were identified by combining the significantly
63 regulated genes across each tumor model ($1.5\times$ and FDR < 0.05 , base mean > 20). Data were
64 analyzed using Ingenuity Pathway Analysis (Qiagen) to obtain the top canonical pathways
65 enriched in the muDX400 DEG set, with the enrichment *P* values depicted in the heatmap.
66 Sample annotations are listed in Table S3.

67 ***Whole exome sequencing***

68 Genomic DNA (gDNA) was extracted from cell lines grown *in vitro* using standard protocols.
69 gDNA was sequenced using the Agilent SureSelect Mouse Exon Kit with 90 base paired end-
70 reads on the Illumina HiSeq 2500. Somatic mutation calling was performed by aligning the
71 whole exome sequencing reads to the mouse reference genome GRCm38 using the BWA-MEM
72 algorithm (2) followed by preprocessing steps including duplicate marking, indel realignment,
73 and base recalibration with Picard (v1.114) and GATK (Genome Analysis Toolkit, version 3.8)
74 (3) to generate analysis-ready BAM files. Somatic mutations were detected using GATK3.7
75 MuTect2 (4) with default parameters by inputting the analysis-ready BAM files of tumor and
76 matched normal tissue (parameter "--dbsnp" was assigned with mouse Single Nucleotide
77 Polymorphism Database [dbSNP]; v150) (5). Variants called by MuTect2 that were present in
78 the dbSNP(v150) were removed. Variants with a mutant allele depth <4 or a total read depth <15
79 were excluded. Variants were annotated with their most deleterious effects on Ensembl
80 transcripts with Ensembl VEP (Variant Effect Predictor, version 86) (6) on GRCm38. Tumor
81 mutational burden was defined as the sum of somatic nonsynonymous variants (including single-
82 nucleotide variants and indels) that passed all the filters described.

83 For neoantigen prediction, mutant 8-11mer peptides that could arise from the identified non-
84 silent mutations in each tumor cell line were identified. If the variant gave rise to a single amino
85 acid change, the mutant peptide was scanned with a sliding window of 8 to 11 amino acids
86 around the variant to generate all possible 8, 9, 10, and 11mers. If the variant created large novel
87 stretches of amino acids that were not present in the reference genome (eg, stop losses or
88 frameshifts), all possible peptides of 8, 9, 10, and 11mers were extracted from the large novel
89 peptide. The binding ability between all the mutant peptides and mouse H2-D, H2-K, H2-L
90 alleles were predicted by netMHC (4.0) (7) with default parameters. For each specific variant,

91 the associated peptides were considered to be neoantigens if the half-maximal inhibitory
92 concentration binding affinity scores of mutant peptides were <500 nM. The number of RNA-
93 sequencing reads covering each of the predicted variants was extracted from the samtools (v1.6)
94 (8) mpileup results (with RNA-sequencing bam files processed by Omicsoft as described above,
95 except that Ensembl.R86 was used as the gene model reference). Neoantigens were considered
96 expressed if both the mutant and the reference alleles were found in ≥ 5 RNA-sequencing reads.

97 **References**

- 98 1. Zhang J, Muise ES, Han S, Kutchukian PS, Costet P, Zhu Y et al. Molecular profiling reveals
99 a common metabolic signature of tissue fibrosis. *Cell Rep Med* 2020;1:100056.
- 100 2. Li H, Durbin R. Fast and accurate short read alignment with Burrows-Wheeler transform.
101 *Bioinformatics* 2009;25:1754-60.
- 102 3. McKenna A, Hanna M, Banks E, Sivachenko A, Cibulskis K, Kernytsky A, et al. The
103 Genome Analysis Toolkit: a MapReduce framework for analyzing next-generation DNA
104 sequencing data. *Genome Res* 2010;20:1297-303.
- 105 4. Cibulskis K, Lawrence MS, Carter SL, Sivachenko A, Jaffe D, Sougnez C, et al. Sensitive
106 detection of somatic point mutations in impure and heterogeneous cancer samples. *Nat*
107 *Biotechnol* 2013;31:213-9.
- 108 5. Sherry ST, Ward M, Sirotkin K. dbSNP-database for single nucleotide polymorphisms and
109 other classes of minor genetic variation. *Genome Res* 1999;9:677-9.
- 110 6. McLaren W, Gil L, Hunt SE, Riat HS, Ritchie GR, Thormann A, et al. The Ensembl Variant
111 Effect Predictor. *Genome Biol* 2016;17:122.
- 112 7. Andreatta M, Nielsen M. Gapped sequence alignment using artificial neural networks:
113 application to the MHC class I system. *Bioinformatics* 2016;32:511-7.
- 114 8. Li H, Handsaker B, Wysoker A, Fennell T, Ruan J, Homer N, et al. The sequence
115 alignment/map format and SAMtools. *Bioinformatics* 2009;25:2078-9.

Table S1. Protein and RNA expression levels of PD-1 and PD-L1

Model	Immunohistochemistry ^a		RNAseq (FPKM_log ₂)						PD-1 Response
	PD-1 Expression	PD-L1 Expression	<i>Pdcd1 (Pd1)</i>			<i>Cd274 (Pdl1)</i>			
			Baseline	Isotype	muDX400	Baseline	Isotype	muDX400	
MC38	Moderate	High	-0.4	1.1	3.7	3.5	3.5	5.6	Highly responsive
MBT2	High	Moderate to very high	3.8	3.8	4.9	3.9	3.6	5.5	Highly responsive
CM3	Moderate	High	1.1	1.1	3.0	5.2	5.1	6.9	Highly responsive
RENCA	Moderate	Very high	2.0	2.7	3.4	4.6	4.3	5.4	Partially responsive
CT26	Moderate to high	Very high	2.7	1.9	3.2	4.9	3.3	4.1	Partially responsive
MB49	Low to moderate	High	1.1	1.2	1.8	4.0	4.2	4.4	Partially responsive
EMT6	Moderate	Low to moderate to high ^b	-1.2	0.0	0.6	3.2	4.2	5.2	Partially responsive
4T1	Low	Low to moderate to high ^b	-1.2	1.3	1.7	3.6	3.8	3.9	Resistant
TC1	Moderate	High	0.7	-0.9	-0.6	3.1	2.3	2.3	Resistant
B16-F10	Low	Low	-2.2	-3.5	-1.8	0.4	0.6	1.6	Resistant
LL/2	Low to moderate	Low	-0.7	-3.8	-2.5	1.2	1.5	1.3	Resistant

Abbreviations: CR, complete response; FPKM, fragments per kilobase million; PD-1, programmed death 1; PD-L1, programmed death ligand 1; TGI, tumor growth inhibition.

^aHighly responsive defined as >70% TGI with multiple CRs), partially responsive defined as 30%-70% TGI with occasional CRs, and resistant defined as <30% TGI.

^bSignificant interspecimen variability.

Table S2. Gene expression changes across 11 syngeneic tumor models. <<See Excel Grid>>

Table S3. Sample details of mice in each syngeneic tumor model <<See Excel Grid>>

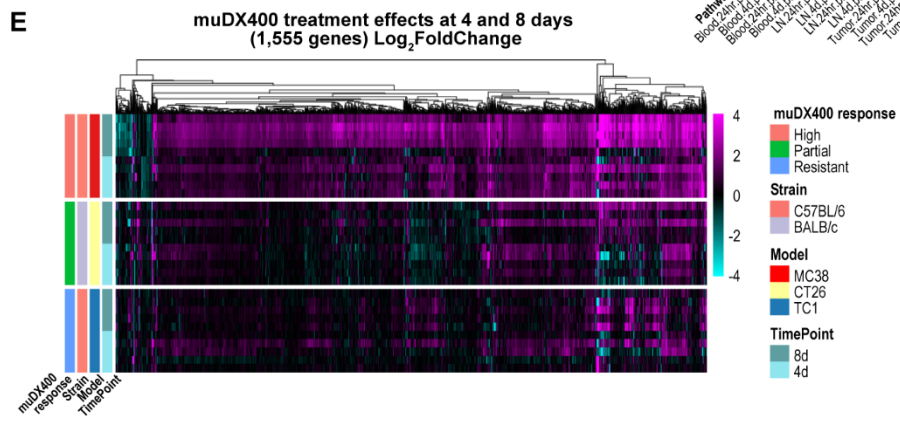
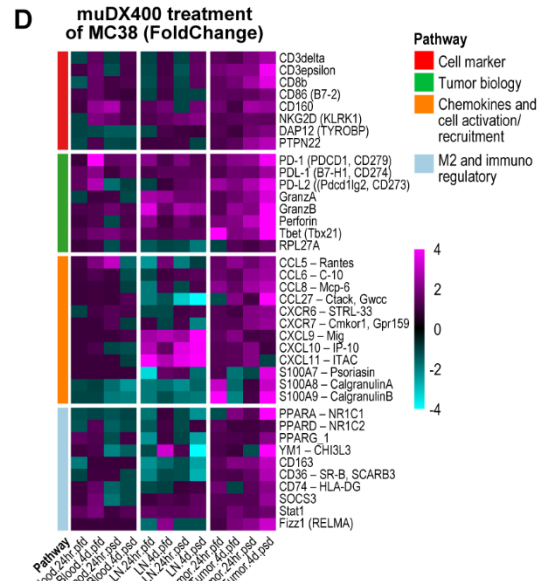
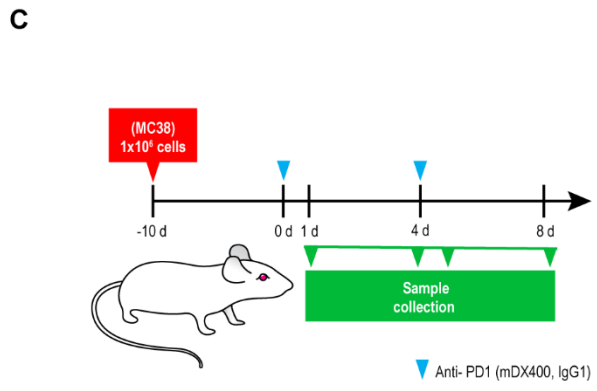
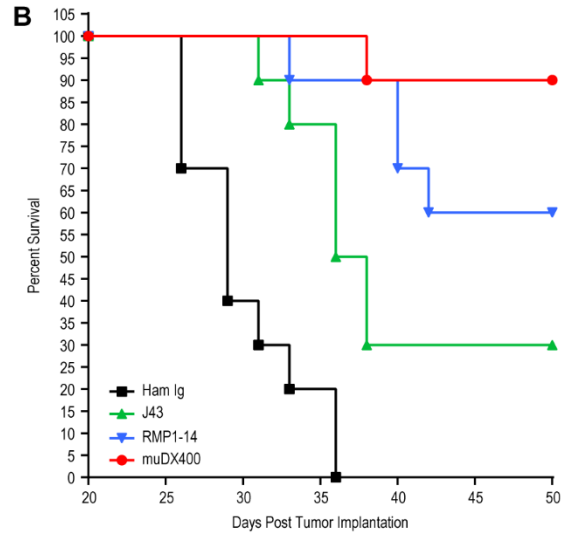
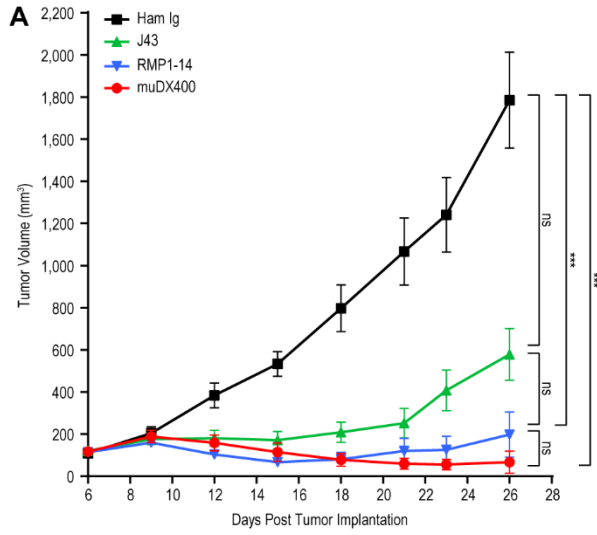


Fig. S1. Comparison of muDX400 in the MC38 model with commercially available anti-PD-1

reagents. A-B, The antitumor activity of muDX400 (muIgG1) was compared with that of the anti-PD-1

clones RMP1-14 (rat IgG2a) and J43 (hamster IgG). Single-agent treatment with 5 mg/kg muDX400 (or

muIgG1 isotype control) began when subcutaneous tumors reached 100 mm³ on average, denoted as day

0. Doses were administered intraperitoneally, with dosing every 5 days for up to five total doses. Tumor

volumes of RMP1-14- and muDX400-treated mice were significantly different from those of isotype

controls ($P < 0.001$) by one-way analysis of variance but not from each other. Similarly, survival between

RMP1-14 and muDX400 was not significant (log-rank test) but was improved over isotype and J43

($P = 0.005$). **C-E,** Time course of gene expression in blood, LN, and tumors of MC38. MC38 tumor-

bearing mice were treated with 5 mg/kg muDX400. **(C)** Blood, LN, and tumor were harvested at 24 hours

and 4 hours after the first dose or the second dose of the antibody. **D,** Samples from three mice were

analyzed with the use of TaqMan Real-Time PCR for a select set of genes. Values were normalized for

expression against housekeeping genes and expressed as fold-change compared with isotype-treated

samples harvested at the same time. **E,** As shown in Fig. 2A, RNA-sequencing of bulk tumors excised

from syngeneic tumor models following single-agent treatment with 5 mg/kg muDX400 or muIgG1

isotype control, 4 days after the first dose or the second dose (see Methods). Shown in the heatmap are the

1555 genes differentially regulated by muDX400 compared with muIgG1 isotype control in any of the

three tumor models shown ($1.5\times$ and $FDR < 0.05$, base mean > 20). The color gradient represents the \log_2 -

fold change of each mouse (each row) treated with muDX400 compared with the corresponding pooled

control mice treated with muIgG1 isotype as baseline ($\pm \log_2$ -fold). Abbreviations: FDR, false discovery

rate; LN, lymph nodes; muIgG1, mouse immunoglobulin G1; PCR, polymerase chain reaction; PD-1,

programmed death 1; Q5D, every 5 days.

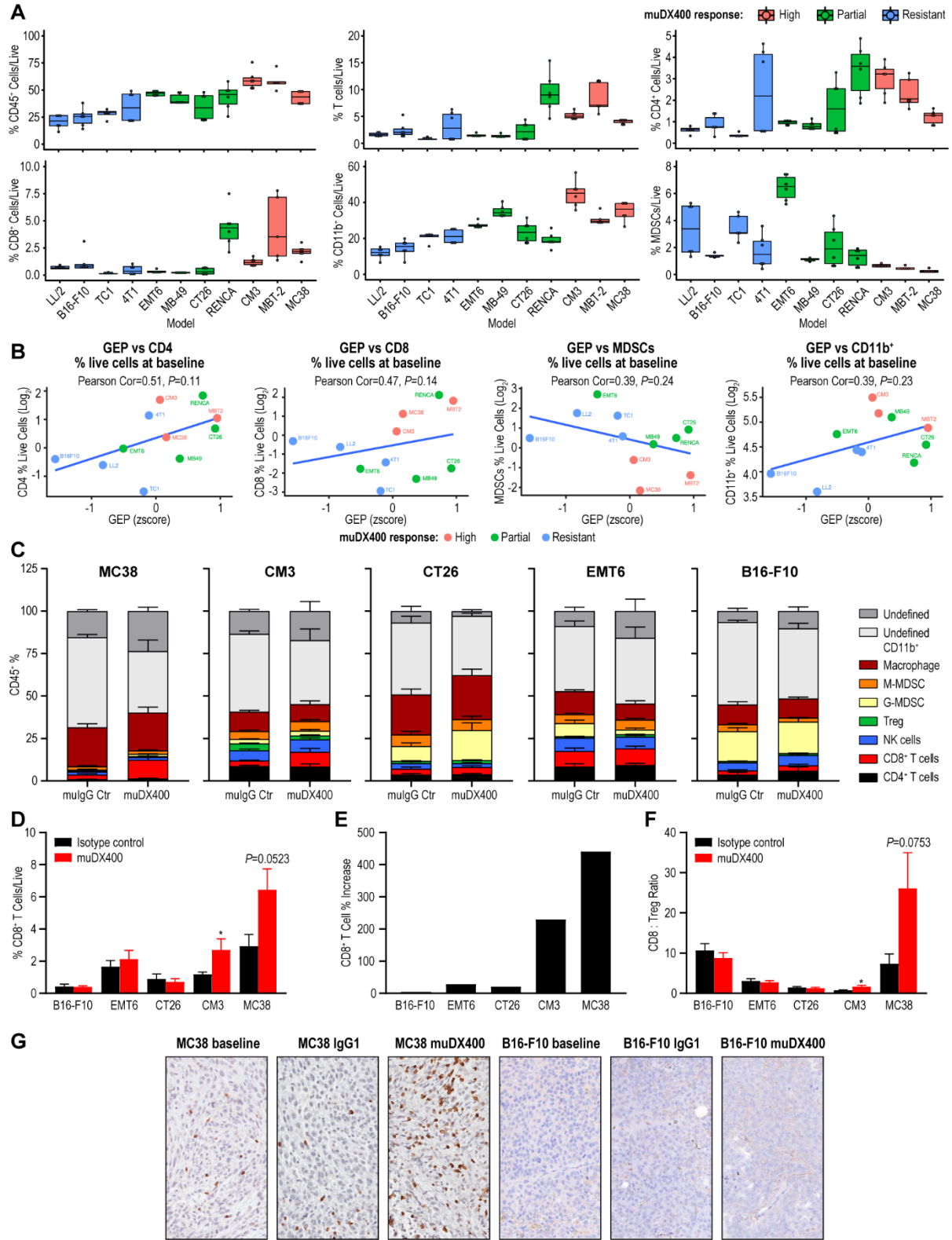


Fig. S2. Immune cell frequencies across differentially responsive syngeneic tumor models at

baseline. Immune infiltrate frequency (as percentage of total live cells) in 100 mm³ tumors was calculated for each syngeneic tumor model. Mice bearing 100 mm³ tumors received two doses (day 0, day 4) of muIgG1 isotype control antibody or muDX400, and tumors were harvested at day 8. Immune infiltrate frequency (as percentage of total live cells) after treatment (day 8) were analyzed. Data are represented as mean \pm SD from a minimum of five tumors and at least two independent experiments for each model. **B,** The 15-gene murine-GEP scores (mean z-scores of the log₂ FPKM values) are plotted against the percentage of various immune cell types among total live cells, at baseline in each tumor model. **C-F,** Mice bearing 100 mm³ tumors received two doses (day 0, day 4) of muIgG1 isotype control antibody or muDX400, and tumors were harvested at day 8. Immune infiltrate frequency (as percentage of total live cells) after treatment (day 8) were analyzed. Frequencies of CD8⁺ T cells, CD8/Treg cell ratio, and CD8 percentage increase following muDX400 or muIgG1 isotype control treatment in the B16-F10, EMT6, MC38, and CM3 syngeneic tumor models. **G,** CD3 expression by immunohistochemistry in the MC38 and B16-F10 models at baseline and day 8 after two doses of muDX400 or muIgG1 isotype control. Data are shown as mean \pm SEM and are from a minimum of five tumors and at least two independent experiments for each model. Abbreviations: GEP, gene expression profile; muIgG1, mouse immunoglobulin G1; SD, standard deviation; SEM, standard error of the mean.

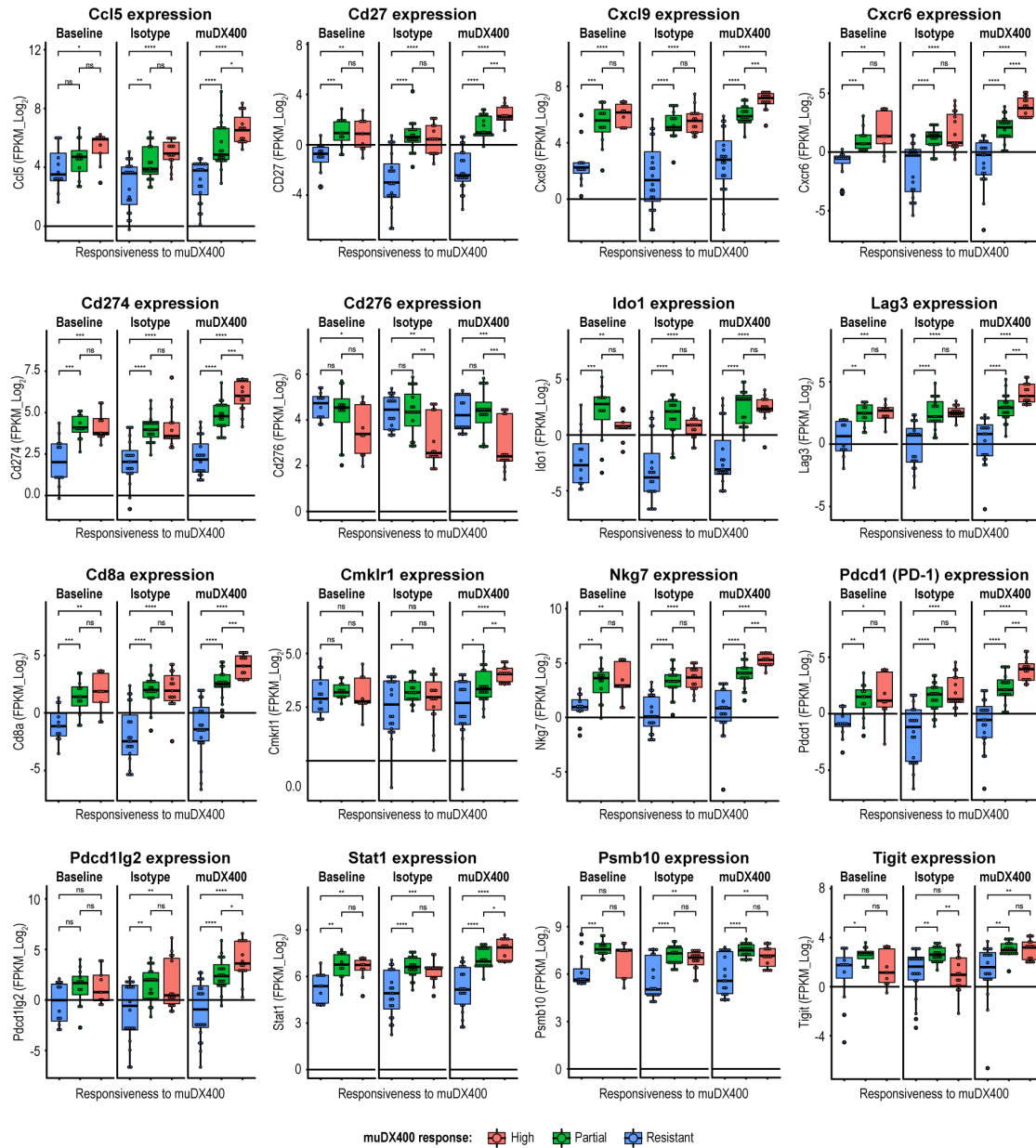
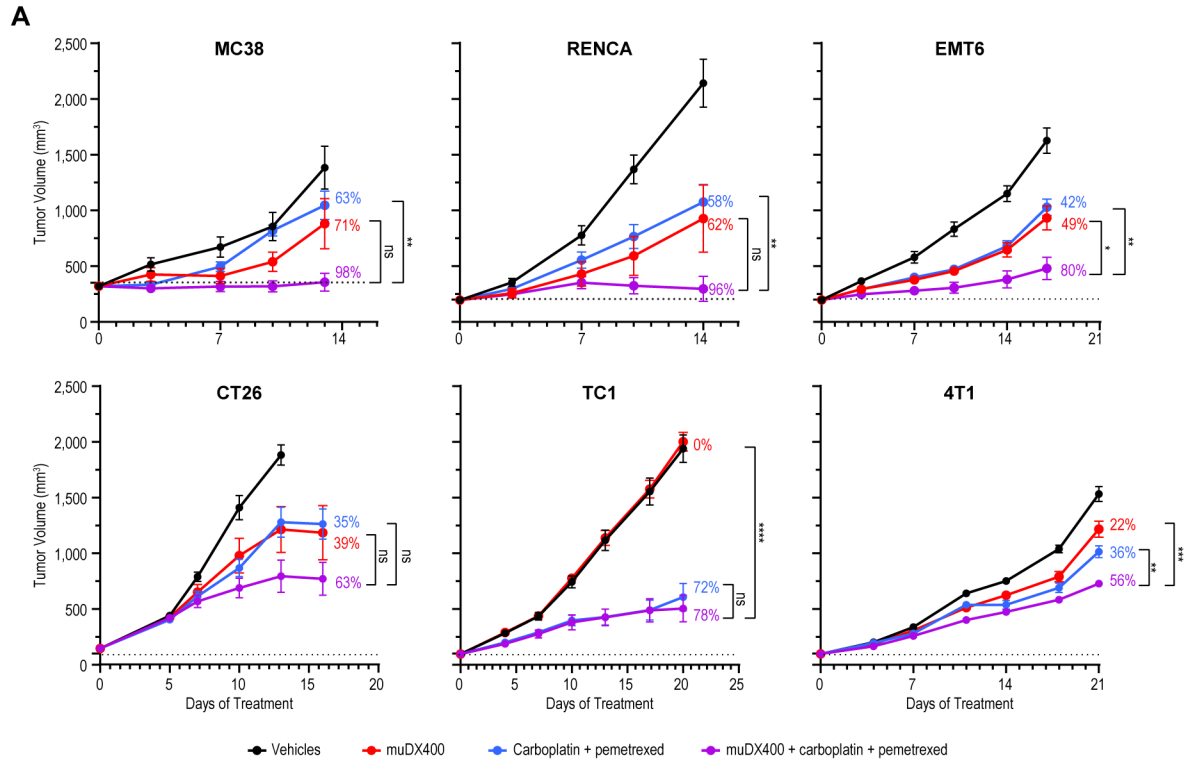


Fig. S3. Expression of the individual murine-GEP genes and *Pdcd1* (*PD1*) across syngeneic tumor models. Boxplots for the 15 murine-GEP genes and *Pdcd1* (*PD1*), depicting the absolute expression levels (FPKM_log₂) across the samples within each tumor model and treatment group. Significance was determined by *t* test (NS, $P > 0.05$; * $P \leq 0.05$; ** $P \leq 0.01$; *** $P \leq 0.001$; **** $P \leq 0.0001$). Abbreviations: FPKM, fragments per kilobase million; GEP, gene expression profile; NS, not significant; PD-1, programmed death 1.



B Chemotherapy combination efficacy summary

Model	CR+PR (%)	SD (%)	PD (%)	TGI (%)	GEP (Z-Score)
MC38	40	20	40	98	-0.04
RENCA	33	22	44	96	0.69
EMT6	20	10	70	80	-0.83
CT26	0	0	100	63	0.94
4T1	0	0	100	56	-0.32
TC1	10	0	90	78	-0.44

CR, complete response (absence of detectable tumor); PR, partial response (>30% tumor shrinkage); SD, stable disease (29% tumor shrinkage, to 19% tumor growth); PD, progressive disease (20% or more tumor growth); TGI, tumor growth inhibition; GEP, 15-gene signature score at baseline.

Fig. S4. Evaluation of PD-1 inhibition and chemotherapy across the syngeneic tumor models. A,

Tumor growth curves for six subcutaneous syngeneic tumor models treated with 5 mg/kg muIgG1 isotype control plus saline, 5 mg/kg muDX400 Q5D, 40 mg/kg carboplatin Q7D plus pemetrexed 200 mg/kg Q7D, or muDX400 and carboplatin plus pemetrexed. Dotted lines represent tumor sizes at the initiation of

treatment. Percentages indicate tumor growth inhibition for each respective treatment regimen. B,

Summary of key parameters of response as shown in A. Data are shown as mean \pm SEM and are representative of at least three independent experiments with $n \geq 10$ mice per group. Statistical significance

was determined by two-way ANOVA with Bonferroni post-test analysis * $P < 0.05$, ** $P < 0.01$,

*** $P < 0.001$, and **** $P < 0.0001$. Abbreviations: ANOVA, analysis of variance; CR, complete response

(tumor not detectable); GEP, gene expression profile; muIgG1, mouse immunoglobulin G1; PD, progressive disease ($\geq 20\%$ tumor growth); PD-1, programmed death 1; PR, partial response ($>30\%$ tumor shrinkage); Q5D, every 5 days; Q7D, every 7 days; SD, stable disease (29% tumor shrinkage to 19% tumor growth); SEM, standard error of the mean; TGI, tumor growth inhibition.